Optimal design of a hydrogen-powered fuel cell system for aircraft applications

Energy Conversion and Management 306 (2024) 118266

Contents lists available at ScienceDirect

Energy Conversion and Management

journal homepage: www.elsevier.com/locate/enconman

Optimal design of a hydrogen-powered fuel cell system for aircraft applications

Maria Chiara Massaro [a], Simone Pramotton [b], Paolo Marocco [b], Alessandro Hugo Antonio Monteverde [a,*], Massimo Santarelli [b]

[a] Department of Applied Science and Technology, Politecnico di Torino, Corso Duca degli Abruzzi 24, 10129 Torino, Italy
[b] Department of Energy, Politecnico di Torino, Corso Duca degli Abruzzi 24, 10129 Torino, Italy

ARTICLE INFO

Keywords:
Hydrogen
Fuel cell
Sustainable aviation
Decarbonization
Electric aircraft

ABSTRACT

Recently, hydrogen and fuel cells have gained interest as an emerging technology to mitigate the effects of climate change caused by the aviation sector. The aim of this work is to evaluate the applicability of this technology to an existing regional aircraft in order to assess its electrification, with the aim of reducing greenhouse gas emissions and achieving sustainability goals. The design of a proton-exchange membrane fuel cell system (PEMFC) with the inclusion of liquid hydrogen storage is carried out. Specifically, a general mathematical model is developed, which involves multiple scales, ranging from individual cells to aircraft scale. First, the fuel cell electrochemical model is developed and validated against published polarization curves. Then, different sizing approaches are used to compute the overall weight of the hydrogen-based propulsion system, in order to optimize the system and minimize its weight. Crucially, this work underscores that the feasibility of hydrogen-based fuel cell systems relies not only on hydrogen storage but especially on the electrochemical cell performance, which influences the size of the balance of plant and especially its thermal management section. In particular, the strategic significance of working with fuel cells at partial loads is demonstrated. This entails achieving an optimal balance between the stacks oversizing and the weights of both hydrogen storage and balance of plant, thereby minimizing the overall weight of the system. It is thus shown that an integrated approach is imperative to guide progress towards efficient and implementable hydrogen technology in regional aviation. Furthermore, a high-performance PEMFC is analyzed, resulting in an overall weight reduction up to nearly 10% compared to the baseline case study. In this way, it is demonstrated as technological advancements in PEMFCs can offer further prospects for improving system efficiency.

1. Introduction

The phenomenon of global warming requires a comprehensive reconsideration of the current energy supply within the transportation sector, particularly regarding aviation, which plays a crucial role. It is of paramount importance to consider the utilization of decarbonized fuels or energy vectors that enable zero-emission propulsion technologies. Since the 1980 s, CO_2 emissions from aviation have increased by 3.6 % per year, twice the overall global growth rate, and are expected to grow by 4.5 % per year [1,2]. Consequently, aviation is currently responsible for 12 % of transport-related CO_2 emissions and for about 5 % of anthropogenic global greenhouse gas (GHG) emissions [3].

In this context, the European Union (EU) has developed multiple strategies to reduce emissions, decarbonize fuels and mitigate the GHGs impact on the upper atmosphere. These strategies include the Fit for 55 package and the Flightpath 2050. The first one concerns a range of revisions and initiatives related to the European Green Deal climate actions and, notably, it aims to achieve a 55 % net emissions reduction compared to 1990 levels. On the other hand, the Flightpath 2050 sets a cut of 75 % in CO_2 emissions and a 90 % decrease in NO_x emissions per passenger, as well as a 65 % reduction of perceived noise [4].

Abbreviations: ***BoP***, Balance of Plant; ***FC***, Fuel cell; ***FCS***, Fuel cell system; ***CCL***, Cathode catalyst layer; ***EM***, Electric motor; ***GDL***, Gas diffusion layer; ***GHG***, Greenhouse gases; ***LH2***, Liquid Hydrogen; ***LHV***, Lower heating value; ***LOHC***, Liquid organic hydrogen carrier; ***MEA***, Membrane electrode assembly; ***MTOW***, Maximum take-off weight; ***NTU***, Number of transfer units; ***ORR***, Oxygen reduction reaction; ***PEM***, Proton exchange membrane; ***PEMFC***, Proton exchange membrane fuel cell; ***RH***, Relative humidity; ***SAF***, Sustainable aviation fuel; ***SOFC***, Solid oxide fuel cell; ***TRL***, Technology readiness level; ***UAV***, Unmanned Aerial Vehicle.

* Corresponding author.
E-mail address: alessandro.monteverdevidela@polito.it (A.H.A. Monteverde).

https://doi.org/10.1016/j.enconman.2024.118266
Received 7 December 2023; Received in revised form 15 February 2024; Accepted 28 February 2024
Available online 18 March 2024

Nomenclature

A_{cell}	Cell area, (cm^2)
$A_{cooling}$	Exchange area for cooling, (m^2)
b	Tafel slope, (V)
c	Oxygen molar concentration, (mol cm^{-3})
c_1, c_2, c_3, c_4	Coefficients for calculation of air properties
c_h	Oxygen concentration in the channel (p = 1 bar), (mol cm^{-1})
C_i	Heat capacity rate of species i, (kW K^{-1})
c_p	Specific heat capacity, (kJ kg^{-1} K^{-1})
c_{ref}	Reference oxygen concentration in the channel, (mol cm^{-1})
D	Effective diffusion coefficient of CCL, (cm^2 s^{-1})
D_b	Effective diffusion coefficient of GDL, (cm^2 s^{-1})
F	Faraday constant, (C mol^{-1})
h	Altitude, (m)
j_*	Exchange current density, (A cm^{-3})
j	Local proton current density in the CCL, (A cm^{-2})
j_0	Cell current density, (A cm^{-2})
j^*_{lim}	Characteristic current density, (A cm^{-2})
l_b	GDL thickness, (cm)
l_t	CCL thickness, (cm)
LHV_{H2}	Lower heating value of hydrogen, (MJ kg^{-1})
$\dot{m}_{air}$	Specific flow rate of air of a single cell, (g s^{-1} cm^{-2})
$\dot{m}_{air,stack}$	Air flow rate fed to a single stack, (g s^{-1})
$\dot{m}_{H2}$	Specific flow rate of hydrogen of a single cell, (g s^{-1} cm^{-2})
$\dot{m}_{H2,stack}$	Hydrogen flow rate fed to a single stack, (g s^{-1})
M_{H2}	Mass of hydrogen, (kg)
$\dot{m}_i$	Flow rate of species i, (kg s^{-1})
MM_{air}	Air molecular weight, (g mol^{-1})
MM_{H2}	Hydrogen molecular weight, (g mol^{-1})
N_{cell}	Number of cells per stack
n_{stack}	Number of stacks
p_{anode}	Working pressure of the fuel cell anode side, (bar)
$p_{cathode}$	Working pressure of the fuel cell cathode side, (bar)
P_{compr}	Electrical power required by the air compressor, (W)
$P_{compr,max}$	Nominal electrical power of the air compressor at stack level, (W)
P_{fc}	Cell power density, (W cm^{-2})
$p_{in,air}$	External air pressure, (bar)
$P_{mission}$	Mechanical power required for the propulsion in a mission, (kW)
$P_{mission,TO}$	Mechanical power required for the propulsion during take-off, (kW)
$P_{stack,max}$	Maximum stack power, (W)
P_{others}	Electrical power required by the auxiliaries, (W)
P_{stack}	Stack electrical power, (W)
$P_{stack,net}$	Net electrical power produced by the stack, (W)
$p_{th,cell}$	Cell thermal power, (W cm^{-2})
Q_{stack}	Heat produced by the stack, (W)
Q_{tot}	Heat produced by the all the stacks, (kW)
R	Heat capacity rate ratio
R_Ω	Area specific resistance, (Ω cm^2)
T	Temperature, (K)
t	Time, (s)
U	Heat transfer coefficient, (kW m^{-2} K^{-1})
V_{cell}	Cell potential, (V)
V_{OC}	Open circuit voltage, (V)
w	Fuel cell working point
w_{compr}	Gravimetric index of compressor, (kW kg^{-1})
$w_{cooling}$	Gravimetric index of cooling system, (kg m^{-2})
w_{EM}	Gravimetric index of electric motor, (kW kg^{-1})
w_{FC}	Gravimetric index of fuel cell stack, (kW kg^{-1})
$w_{H_2storage}$	Gravimetric index of storage system, (kg_{H2} $kg^{-1}_{storage\ system}$)
W_{tot}	Total weight of electrified propulsion system, (kg)
x	Coordinate across the CCL, (cm)
y_{O2}	Molar fraction of oxygen in air
y_{others}	Fixed parameter for auxiliaries power requirement

Subscripts

0	Membrane/CCL interface
air	Air property
b	GDL
comp	compressor
coolant	Coolant property (Glysantin)
h	Channel
in	inlet
out	outlet
t	Catalyst layer
*	Characteristic value

Greek

β	Dimensionless parameter, a function of j_0
β_{compr}	Compression ratio
γ	Adiabatic exponent of air
$\Delta\bar{h}_{react}$	Molar enthalpy of reaction occurring in the cell, (J/mol)
ε	Effectiveness of radiator heat exchange
η	Local overpotential, (V)
η_{cell}	Cell efficiency
η_{em}	Electromechanical efficiency of compressor
η_{EM}	Electromechanical efficiency of electric motor
η_{is}	Isentropic efficiency of compressor
η_{net}	Efficiency of the system
λ_{air}	Air excess fed in cell
λ_{H2}	Hydrogen excess fed in cell
σ_t	Proton conductivity in the catalyst, (S cm^{-1})

In the last three decades, the aviation sector has significantly improved carbon efficiency per passenger. Optimization strategies, including increased seat density and utilization, along with operational and technological enhancements, have played a significant role in this improvement [5]. Additionally, retrofitting options for existing aircraft, such as the integration of blended winglets, cabin weight reduction, electric taxing, and reengining, have demonstrated the potential to achieve a notable fuel consumption reduction ranging from 9 to 12 % [6]. However, the current attempts to reduce CO_2 emissions are not enough to offset the growth in the aviation sector and meet the sustainability goals. To comprehensively address these challenges, a multifaceted approach is crucial. In addition to ongoing optimizations and retrofits, integrating sustainable aviation fuels (SAFs), enhancing air traffic management, and continuous research into greener technologies are imperative [5].

Examining the automotive industry as a benchmark in the transportation sector, it is evident that the favored approach is towards electrification to achieve emission reduction targets. The concept of aircraft electrification has attracted academic and industry interest over the past decade, leading to a surge in literature in the field and the creation of several start-up companies aiming to commercialize electric aircraft propulsion systems: full electric aircraft could avoid not only all air pollutants but mostly direct CO_2 emissions [7,8].

The implementation of the new propulsion system necessitates a

careful selection of the source of energy on-board the aircraft. Currently, the most promising technologies in this regard are hydrogen as fuel and fuel cells (FCs) as converters [9]. Even if batteries demonstrate excellent roundtrip efficiency, acceptable power density (under on-ground conditions), and a high technological readiness level (TRL), they appear unsuitable for the aviation sector, particularly for fuel-intensive aircraft such as long-haul planes. This is primarily due to their low gravimetric energy densities (ranging between 0.2 and 0.5 kWh/kg) and limited lifetime cycles. For such applications, hydrogen exhibits a great potential owing to its gravimetric energy density of 33.3 kWh/kg, which is three times higher than kerosene and more than 100 times higher than batteries. However, on-board storage of hydrogen in aircraft remains challenging due to the low volumetric energy density of hydrogen, which requires larger tanks and adjusted aircraft designs [5,9]. At the same time, the enhanced efficiency of fuel cells contributes to a reduction in fuel load compared to conventional kerosene-based configurations [10]. Fuel cells offer additional advantages for electric aircraft, such as distributed propulsion, which improves aerodynamic efficiency. Moreover, the multifunctional integration of the fuel cell into the aircraft, through the recovery of by-products such as water, heat or oxygen-depleted exhaust air, allows the fuel cell to be used for vital processes such as de-icing, cabin air conditioning, water supply or firefighting in the baggage compartment or fuel tanks [11].

In addition, the concept of electric aircraft can lead to greener air transport for two other reasons [12]. Firstly, unlike the gas turbine, the electric propulsion is not bound by the limits in efficiency of thermal machines (Carnot limit) and has the potential to achieve higher efficiency in on-board energy conversion [13]. Secondly, these aircrafts would probably use a system of electric motor-driven fans, whose efficiency scales better with size than that of gas turbines [14].

However, stringent requirements exist for an airborne application, including weight reduction, safety, and reliability. These aspects imply important challenges for the integration of fuel cell solutions in an aircraft, such as maintaining the weight and balance of the aircraft, managing the waste heat, storing hydrogen efficiently and ensuring a safe operation [15,16].

Numerous studies have approached the challenge of aircraft electrification from various perspectives. Some investigations have been specifically devoted to optimizing the balance of plant (BoP), which is critical in hydrogen-powered fuel cell systems. These studies involve analyzing innovative cooling strategies, as well as fine-tuning parameters such as temperature and pressure. Kösters et al. [16] proposed a novel phase-change-heat-pump (PCHP) cooling strategy to significantly enhance the specific power of fuel cell systems in aviation. The study quantifies the potentials of the PCHP cooling concept by evaluating its impact on aerodynamic and weight-induced drag. Finally, the study explores possible synergies between cooling solutions and fuel cell operation, emphasizing the quantification and comparison of parasitic drag power consumption between the PCHP cooling system and the conventional liquid-cooling system. Lee et al. [17] analyzed the impact of air pressurization in an air-cooled fuel cell system, showing the trade-off between fuel cell stack power improvement and parasitic power consumption by air pressurization and recirculation. HyPoint company has developed an innovative system configuration based on an air-cooled high-temperature proton exchange membrane fuel cell (PEMFC), operating at temperatures between 160 and 180°C. By adopting this approach, the company asserts a noteworthy 61 % reduction in the weight of the FC system compared to a liquid-cooled low-temperature PEMFC [11].

Concurrently, substantial efforts are directed towards improvements in hydrogen storage and on-board installation. In fact, the shift to hydrogen introduces complexities, influencing aircraft weight, structure, and cost, highlighting the need for careful consideration and optimization in the integration of hydrogen-powered aviation [9]. In this context, Massaro et al. [11] analyzed the potential and the technical challenges of hydrogen-powered fuel cells for aircraft electrification and proposed a detailed comparison of several hydrogen storage technologies and a preliminary sizing of the electric propulsion system. The work showed that liquid and cryo-compressed hydrogen are the most promising solutions for on-board storage due to the higher gravimetric density and the easier and more compact hydrogen delivery. Metal borohydrides, liquid organic hydrogen carriers (LOHCs) and ammonia were also mentioned as interesting storage methods that have great potential for future development due to their currently low TRLs. Kadyk et al. [18,19] explored the application of fuel cells and hydrogen in aviation in two scientific papers, both published in 2018. In the first one, they discussed the design of hydrogen storage systems for future aircraft applications. In particular, they formulated a model for the design of the cryogenic tank that takes into account geometric, mechanical and thermal aspects as well as specific mission profiles considering a fuel cell power supply [18]. In the second paper, they focused on the design of the fuel cell system, starting from the electrochemical model of a single fuel cell [19]. Recently, the Center for High-Efficiency Electrical Technologies for Aircraft (CHEETA) program, sponsored by NASA in the United States, investigated the cryogenic flow circuit of all-electric aircraft and the design of storage tank walls. The study focused on exploring different designs for liquid hydrogen storage, incorporating an outer tank, a vacuum space, and an inner liquid hydrogen tank in each configuration. Finally, the identification and selection of the lightest weight design that provides sufficient safety margins against two failure modes were carried out, deeming it suitable for practical application [20]. Adler at al. [21] conducted a comprehensive review on hydrogen-powered aircraft, further highlighting key considerations in liquid hydrogen storage. They emphasize the significance of maintaining a low surface area-to-volume ratio in tank design to mitigate heat infiltration into the fuel. Furthermore, the study underscores the pivotal role of thermal insulation in minimizing boil-off, emphasizing the need for materials capable of withstanding cryogenic temperatures. Achieving a delicate balance between reducing insulation weight and adhering to operational constraints emerges as a critical factor in determining the optimal amount of boil-off for these advanced liquid hydrogen storage systems.

Other works had a strong focus on overall system design aspects and on-board integration. Guida et al. [15] implemented a mathematical tool for designing a fuel cell power supply system powered by liquid hydrogen. The approach is based on the optimization of each system component in order to achieve the highest specific energy value of the power unit. Nicolay et al. [22] proposed a new design approach for sustainable general aviation, distinct from retrofit designs. The objective was to optimize the entire aircraft configuration, considering components such as liquid hydrogen tanks, fuel cells, electric motors, as well as passenger seats and cargo hold. Sparano et al. [10] presented a model-based preliminary design methodology for a hybrid regional aircraft assisted by a battery-hybridized fuel cell powertrain, introducing a control strategy that meets the specific needs of the aeronautical application.

The multi-approach investigation on hydrogen fuel cells for aviation reflects the multifaceted nature of integrating such systems on-board the aircraft. Advancements in both auxiliary systems and core fuel cell technologies are indispensable for achieving sustainable and efficient electrification of airborne systems.

The use of fuel cell and hydrogen in aviation applications is already being tested in demonstration projects across different use cases. However, due to the unique challenges posed by aviation (i.e., extremely large energy demands), projects to date focus on light small-scale Unmanned Aerial Vehicles (UAVs) and passenger airplanes (less than 5 passengers) [10]. For example, in 2023 a significant milestone was reached with the successful completion of the world's first piloted flight of a liquid hydrogen-powered electric aircraft, realized within the European government-supported HEAVEN project led by H2FLY [23]. ZeroAvia is actively involved in the development of a customized hydrogen fuel cell propulsion system for aviation, with the aim of

commercializing a 9–19 seat electric aircraft with 300 NM range, fueled by gaseous hydrogen tanks, by 2025 [24].

Contrary to existing literature, the present work introduces an integrated methodology that encompasses multiple scales (ranging from individual cells to aircraft scale) to address the efficiency of the proposed propulsion system, a parameter intrinsically linked to the specific mission profile of the aircraft. This approach offers a comprehensive but precise methodology that allows for the consideration of potential technological advancements in individual system components and their impact on the overall system size.

Specifically, the present work aims to advance the analysis and design of the fuel cell system and integrate it with the hydrogen storage design. The distinctive feature of this work is that the electrochemical model of the fuel cell was exploited to size the components of the propulsion system and optimize their operation, minimizing the overall weight of the system. Numerical methods were employed to validate the model-generated curves by comparing them with experimental data, and the efficiency of the fuel cell system was adapted to the mission profile of the aircraft. The whole design process was applied to a commercial regional aircraft, considering its mission profile. A comparative analysis between the current propulsion system and the designed electric propulsion system was conducted, and potential future improvements were evaluated to recalculate the sizing and achieve the technical requirements.

2. Methodology

This section illustrates the methodology adopted to calculate the size of a full hydrogen-based propulsion system for an all-electric aircraft. All calculations were carried out using MATLAB and the associated tools. The calculation procedure unfolds across three distinct levels: individual electrochemical cell, fuel cell system, and aircraft system.

First, the appropriate technology for both the fuel cell and the onboard hydrogen storage was selected. This step was crucial for identifying and designing the components of the propulsion system.

Proton exchange membrane fuel cell was chosen as technology of conversion because of its suitability for transport applications [25], while a cryogenic tank was selected for the hydrogen storage in its pure liquid form, because of its good gravimetric density [11]. Both technologies are characterized by a high TRL among hydrogen technologies, with a consequent reliability for short-term application.

Regarding the design of the fuel cell, there are two viable options. The first option involves selecting an existing commercial PEMFC stack and conducting the sizing analysis based on its available technical data. This was the strategy adopted by the same research group for a previous feasibility study [11]. The limitation of the approach just described is that the selected fuel cell is already a well-established commercial product; consequently, it restricts the ability to make significant modifications and evaluate the impact of new solutions or optimizations on the overall performance of the fuel cell. The second option, which was selected for the present study, involves developing an electrochemical model that accurately reproduces the physical behavior of an individual cell. This model is then validated with real technology data, subsequently scaled up for the sizing process and used to analyze technical solutions for improvement of the FC-based powertrain.

The initial step was to establish an electrochemical model of a single cell that comprehensively describes all the multi-physical phenomena occurring within the cell, enabling the determination of its polarization curve, power curve, and efficiency curve. Once these characteristics were achieved, the scaling up to the stack level was carried out, beginning with a predefined geometric structure. Finally, the complete propulsion system was sized, considering a sufficient number of stacks and the relative balance of plant.

2.1. Electrochemical model of single cell

The electrochemical model of the single cell consists of a set of equations that simulate the most relevant transport phenomena occurring within the fuel cell. This model provides results in terms of polarization curve, as well as power and efficiency curves. Additionally, it enables the calculation of reactant flow rates and thermal power to be removed, which are fundamental input for the sizing of the BoP.

2.1.1. Electrochemical model description

The electrochemical analysis of the single cell is based on a PEMFC model developed by Andrei Kulikovsky [26]. The model allows for obtaining a simplified but accurate analytical solution by incorporating the most relevant processes occurring within the cell. These processes are described in a simple manner, considering physically meaningful, macroscopic parameters.

The model has three main advantages:

1. the functional relationship between parameters and interesting variables is directly revealed;
2. the model has no computational limitations and can be included into larger model hierarchies, e.g., for aircraft design, aircraft fleet models or future aviation scenario modelling;
3. the effective, physical parameters can be used to estimate potential improvements due to future materials' development.

In the model, the main losses of the fuel cell system come from the cathode catalyst layer (CCL), while the anode losses are considered negligible [19].

For the cathode performance, a well-known model based on pioneering works of Perry, Newman and Cairns [27] as well as Eikerling and Kornyshev [28] was used.

The CCL model is one-dimensional (1D) in through-plane direction, steady-state and isothermal, and it consists of the governing equations reported in Table 1.

Since the diffusion coefficients in CCL and GDL (i.e., D and D_b, respectively) are effective parameters, polarization curves for flooded conditions can be simulated. However, a changing water balance (i.e., a dependency of the diffusion coefficients on current) was not modelled in detail here.

Under these assumptions, Kulikovsky was able to obtain the analytical solution for the polarization curve $\eta_0(j_0)$, which is valid for large overpotentials, $\eta_0 \gg b$:

$$\eta_0 = arcsinh\left(\frac{(j_0/j_\sigma)^2}{2(c_h/c_{ref})(1-exp(j_0/2j_*))}\right) + \frac{\sigma_t b^2}{4FDc_h}\left(\frac{j_0}{j_*} - ln\left(1 + \frac{j_0^2}{j_*^2\beta^2}\right)\right)\left(1-\frac{j_0}{j_{lim}^*(c_h/c_{ref})}\right)^{-1} - b\,ln\left(1-\frac{j_0}{j_{lim}^*(c_h/c_{ref})}\right) \quad (4)$$

with three characteristic current densities:

$$j_* = \frac{\sigma_t b}{l_t} \quad (5)$$

Table 1
Governing equations used for the one-dimensional, through-plane model of the single PEM fuel cell.

Phenomenon	Governing equation	
Rate of the oxygen reduction reaction (ORR) in CCL	$\frac{dj}{dx} = j_*\left(\frac{c}{c_{ref}}\right)exp\left(\frac{\eta}{b}\right)$	(1)
Ohm's law for proton conduction	$-\sigma_t\frac{d\eta}{dx} = j$	(2)
Oxygen diffusion through gas diffusion layer (GDL) and CCL	$D\frac{dc}{dx} = \frac{j_0 - j}{4F}$	(3)

$$j_\sigma = \sqrt{2 i_* \sigma_t b} \tag{6}$$

$$j_{lim}^* = \frac{4FD_b c_h}{l_b} \tag{7}$$

where l_t and l_b are the thickness of CCL and GDL, respectively. The parameter β is a solution to the equation below:

$$\beta tan(\beta/2) = j_0/j_* \tag{8}$$

and can be accurately approximated by

$$\beta = \frac{\sqrt{2(j_0/j_*)}}{1+\sqrt{1.12(j_0/j_*)}exp\left(\sqrt{2(j_0/j_*)}\right)} + \frac{\pi(j_0/j_*)}{2+(j_0/j_*)} \tag{9}$$

The first term on the right-hand side of Equation (4) characterizes the overpotential due to the combined effect of ORR activation and proton transport, while the second and the third terms describes the potential losses due to oxygen transport in the CCL and in the GDL, respectively.

The cell voltage (in V) was calculated as the difference between the open circuit voltage and the overpotential losses contributions:

$$V_{cell}(j_0) = V_{oc} - R_\Omega j_0 - \eta_0 \tag{10}$$

In this model, the cross-over effects on the V_{oc} were neglected, even if they could be easily implemented in the model.

For the validation of the model, some parameters were adjusted during the curve fitting process, considering their physical reliability:

- the volumetric cathode exchange current j_*, which influences mainly activation losses, is strictly linked to the catalyst loading and can vary generally from $1 \cdot 10^{-3}$ to $4 \cdot 10^{-2}$ A cm^{-3} [29];
- the GDL thickness l_b, which influences mostly the concentration losses, can vary generally from 0.015 to 0.04 cm [30];
- the conductivity D in the CCL, which evenly influences the concentration losses with the mass transport limitation, can vary generally from $1 \cdot 10^{-4}$ to $3 \cdot 10^{-4}$ cm^2 s^{-1} [26];
- the ohmic resistance R_Ω, which influences mainly ohmic losses and involves both ionic and electrical resistance, can vary generally from 0.2 to 0.045 Ω cm^2 [31].

2.1.2. Mass balance

The specific hydrogen flow rate $\dot{m}_{H2}$ (in g s^{-1} cm^{-2}) was calculated from the Faraday's law as function of the cell's current density (j_0) and the hydrogen excess (λ_{H2}), and taking into account the molecular mass of hydrogen (MM_{H2}):

$$\dot{m}_{H2}(j_0) = \lambda_{H2}\frac{j_0}{2F}MM_{H2} \tag{11}$$

In the present case study, the excess of hydrogen was imposed equal to 1, because it was supposed a complete recirculation of the outlet hydrogen flow rate.

The specific air flow rate $\dot{m}_{air}$ (g s^{-1} cm^{-2}) was calculated in a similar way, considering the Faraday's law for oxygen, its concentration in the air (y_{O2}), the excess of air fed into the cell (λ_{air}) and the molecular mass of air (MM_{air}):

$$\dot{m}_{air}(j_0) = \frac{\lambda_{air}}{y_{O2}}\frac{j_0}{4F}MM_{air} \tag{12}$$

2.1.3. Power density and efficiency

After validating the polarization curve, the power and efficiency curves of the fuel cell were calculated. The electrical power density (W cm^{-2}) of the cell is expressed as

$$P_{fc}(j_0) = V_{cell}(j_0) j_0 \tag{13}$$

while the electrical efficiency of the cell is

$$\eta_{cell}(j_0) = \frac{P_{fc}(j_0)}{\dot{m}_{H2}(j_0) LHV_{H2} 10^3} \tag{14}$$

The specific heat released per cell during the FC operation (W cm^{-2}) can be computed as follows:

$$p_{th,cell}(j_0) = j_0\left(\frac{-\Delta\bar{h}_{react}}{2F} - V_{cell}(j_0)\right) \tag{15}$$

where $\Delta\bar{h}_{react}$ is the molar enthalpy of reaction, which was assumed constant with the operating temperature and equal to −286,000 J mol^{-1}.

2.2. Fuel cell system

The fuel cell system is composed by the electrochemical stack surrounded by a series of components that constitute its BoP and play a crucial role in managing the stack itself. Fig. 1 illustrates the control volume, regarded as the repetitive unit for the sizing of the fuel cell system, consisting of the stack and the most impactful components of its BoP. Detailed descriptions of these components are provided in the present section.

2.2.1. Fuel cell stack

The stack was designed by considering the performance of the single cell and defining its area and the number of cells from a reference geometrical stack structure [32], as reported in Table 2. The assumption underlying the design of the stack is that it exhibits similar performance to that of the single cell. This approximation is justified by the primary objective of the present paper, which is to conduct a preliminary feasibility study. In this context, the focus has been on assessing the fundamental viability of the proposed system, and as such, it was not explicitly accounted for the distribution of water and temperature within the stack.

From the stack features, it was possible to determine all the input/output quantities referred to the stack: voltage, current, electrical and thermal power, reactant flow rates.

In particular, the power (in W) produced by the stack was computed as:

$$P_{stack}(j_0) = P_{fc}(j_0) N_{cell} A_{cell} \tag{16}$$

The flow rate of air at stack level ($\dot{m}_{air,stack}$) was computed in a similar way based on the value at the cell level (Equation (12)). Similarly, the flow rate of hydrogen sent to a single stack ($\dot{m}_{H2,stack}$) was derived from the cell-level term (Equation (11)).

2.2.2. Balance of Plant: Energy-intensive components

The main energy-demanding components of the BoP were identified and sized in relation to their power requirements. Indeed, these components are powered directly by the fuel cell, underscoring the significance of accurately sizing them to determine the gross power output needed from the stack, as well as the resulting stack size.

The power absorbed by the auxiliary units is divided into two different contributions:

- the compressor absorbs a large variable amount of power;
- others: absorb a small, fixed amount of power.

The power consumption of the air compressor (in W) was calculated under adiabatic conditions with fixed efficiency. Hence, the equation of the power absorbed by the compressor was used.

$$P_{compr}(j_0, h) = \dot{m}_{air,\,stack}(j_0) c_{p,air} T_{in,air}\left(\beta_{compr}^{\frac{\gamma_{air}-1}{\gamma_{air}}} - 1\right)\frac{1}{\eta_{is}}\frac{1}{\eta_{em}} \tag{17}$$

In order to calculate the power consumed by the compressor, some pa-

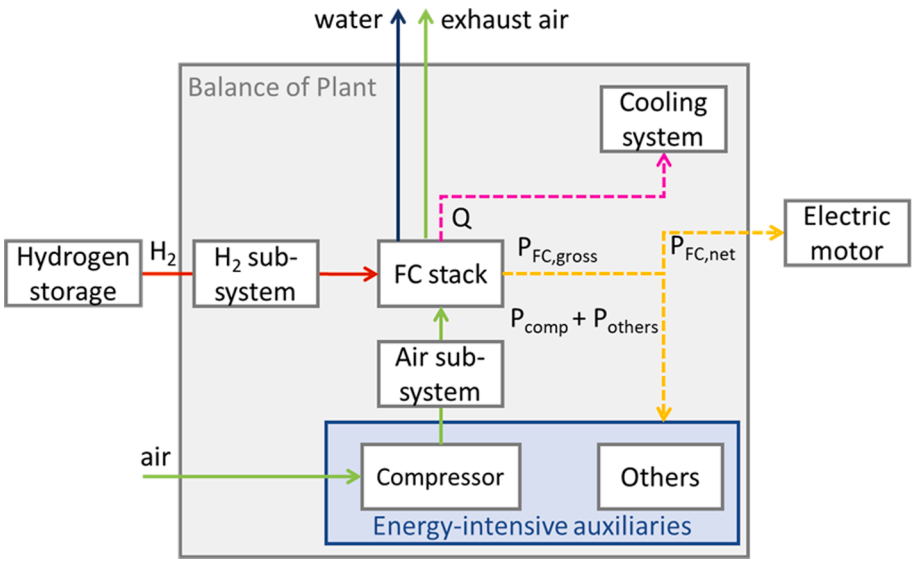

Fig. 1. General layout of the propulsion system of the hydrogen-powered aircraft, which includes: hydrogen storage, fuel cell system (FCS) and electric motor [11].

Table 2
Stack features.

Parameter	Value	Unit	Description	Reference
N_{cell}	309		Cells per stack	[32]
A_{cell}	480	cm^2	Area of the cell	[32]

rameters must be set, first of all the air intake conditions. In particular, the inlet temperature $T_{in,air}$ and pressure $p_{in,air}$ are both function of the altitude (h). The first one drops linearly, the second one drops exponentially with the following laws:

$$T_{in,air} = 288.19 - 0.00649h \tag{18}$$

$$p_{in,air} = 1.0129\left(\frac{T_{in,air}}{288.08}\right)^{5.256} \tag{19}$$

where h indicates the altitude and is in meters, $p_{in,air}$ is in bar and $T_{in,air}$ in K.

It should be noted that altitude varies during flight and is the most important variable for the calculation of the auxiliaries. The increase in altitude has a double effect on the specific power absorbed by the compressor: the drop in pressure leads to an increase in the compression ratio and consequently in the absorbed power, while the decrease of temperature has the opposite effect. The first factor is more influential than the second, leading to an increase in absorbed power with altitude.

To obtain a final conservative design, the maximum cruising altitude was chosen, i.e., the worst condition for compressor operation was considered.

The adiabatic exponent (γ_{air}) and the specific heat of the air ($c_{p,air}$, in kJ kg^{-1} K^{-1}) were calculated as a function of the air temperature ($T_{in,air}$, in K), by performing a fitting process of thermophysical data [33]. The coefficients of the fitting equations are resumed in Table 3.

Table 3
Thermophysical coefficients for the estimation of the adiabatic exponent and the specific heat of air.

Parameter	Value	Value
	$c_{p,air}$ [kJ kg^{-1} K^{-1}]	γ_{air} [-]
c_1	$-3.612 \cdot 10^{-10}$	$1.877 \cdot 10^{-10}$
c_2	$7.897 \cdot 10^{-7}$	$-3.837 \cdot 10^{-7}$
c_3	−0.0003288	0.0001469
c_4	1.0417	1.385

$$c_{p,air} = c_1 {T_{in,air}}^3 + c_2 {T_{in,air}}^2 + c_3 T_{in,air} + c_4 \tag{20}$$

$$\gamma_{air} = c_1 {T_{in,air}}^3 + c_2 {T_{in,air}}^2 + c_3 T_{in,air} + c_4 \tag{21}$$

Finally, the compression ratio β_{compr} was calculated as the ratio between air pressure at the compressor inlet (i.e., external air pressure) and cathode pressure:

$$\beta_{compr} = \frac{p_{cathode}}{p_{in,air}} \tag{22}$$

By considering the power requirement of the compressor as function of current and altitude, the compressor size at stack level ($P_{compr,max}$) was determined.

The power consumption of the other auxiliary units was modelled as a fixed term called P_{others}, which represents the power consumption of all small equipment such as pumps, valves, control units that are constantly in operation. This was evaluated with a fixed percentage of the maximum power of the stack:

$$P_{others} = y_{others} P_{stack,max} \tag{23}$$

where y_{others} is a constant value set to 1% [11] and $P_{stack,max}$ is the maximum power of the stack, calculated through Equation (16) in the maximum power point.

2.2.3. Balance of Plant: Cooling system

The thermal power generated by the stack, denoted as Q_{stack} (in W), which is function of the current density j_0, was derived from the heat of the single cell, as follows:

$$Q_{stack}(j_0) = p_{th,cell}(j_0) N_{cell} A_{cell} \tag{24}$$

This parameter was crucial for determining the size of the cooling system in the subsequent step of aircraft-scale dimensioning of fuel cell system.

The designed cooling system consists of a closed circuit where a liquid coolant is used to cool the stack and then returns to its initial temperature conditions through an air radiator.

In particular, the initial assumptions were:

- the liquid coolant is Glysantin [34];

Table 4
Input parameters for the model of the fuel cell system.

Component	Parameter	Value	Unit	Description
FC stack	$p_{cathode} = p_{anode}$	1.5	bar	Working pressure of the fuel cell [35,36]
	λ_{air}	2	–	Air molar excess respect to stoichiometry [37,38]
	λ_{H2}	1	–	Hydrogen molar excess respect to stoichiometry
Compressor	η_{is}	0.75	–	Isentropic efficiency
	η_{em}	0.95	–	Electro-mechanic efficiency
Auxiliaries	y_{others}	1	%	Percentage of nominal fuel cell power for general auxiliaries [11]
Cooling system	$T_{in,coolant}$	70	°C	Inlet temperature of FC coolant
	$T_{out,coolant}$	80	°C	Outlet temperature of FC coolant (equal to FC operative temperature)
	$c_{p,coolant}$	3.55	kJ kg^{-1} K^{-1}	Specific heat capacity of coolant [34]
	$T_{in,air}$	40	°C	Inlet temperature of air in the radiator
	$T_{out,air}$	55	°C	Outlet temperature of air from the radiator
	$c_{p,air}$	1.005	kJ kg^{-1} K^{-1}	Specific heat capacity of air
	$t_{coolant}$	10	s	Circulation time of liquid coolant into the circuit [39]
	U	0.1	kW m^{-2} K^{-1}	Heat transfer coefficient

- the liquid coolant water exits the fuel cell at the same operative temperature of the stack;
- the air at the inlet of the radiator, which is the external air, has a sizing temperature of 40°C;
- the variation of the coolant temperature is equal to 10°C;
- the variation of the cooling air temperature is equal to 15°C.

2.2.4. Net power and system efficiency

The net electrical power $P_{stack,net}$ of the fuel cell system was calculated as a function of both the operative current and the mission profile, considering the power provided to the compressor and the other auxiliaries:

$$P_{stack,net}(j_0, h) = P_{stack}(j_0) - P_{comp}(j_0, h) - P_{others} \quad (25)$$

This step was crucial for the subsequent sizing of the propulsion system at the aircraft level. Indeed, the number of stacks was determined based on the net power that each stack can supply to the electric motor.

Finally, starting from the stack net power, the efficiency curve of the fuel cell system was defined as function of the operative current and altitude.

$$\eta_{net}(j_0, h) = \frac{P_{stack,net}(j_0, h)}{\dot{m}_{H2,stack}(j_0) LHV_{H2} 10^3} \quad (26)$$

2.2.5. Input parameters

Table 4 reports the input parameters imposed for the design of the fuel cell system.

2.3. Sizing criteria

The successive step was to model the propulsion system of the full hydrogen-powered aircraft. This model identifies three different main sections: the hydrogen tank, the fuel cell system (including stacks and BoP) and the electric motor. The general layout of the entire FC-based propulsion system is shown in Fig. 1.

The commercial regional aircraft ATR72-600, whose specifics are summarized in Table 5, was selected for the sizing of the propulsion system. As indicated in Table 5, the maximum take-off weight (MTOW) of the selected aircraft is 22.8 tonnes, which is divided into the following components: structure, payload, propeller and kerosene-based propulsion system [11]. The latter term includes a thermal engine per half-wing, the fuel (i.e., kerosene) and the relative storage system.

The sizing consisted of calculating the number of stacks required for the FCS, the exchange area of the cooling system, and the mass of hydrogen required for the hydrogen tank. For this purpose, the working point of the stack was selected. Then the weights of the devices were calculated via:

- the specific power (kW kg^{-1}) for the stacks, compressor and electric motor;
- the gravimetric density for the hydrogen tank;
- the gravimetric specific area (m^2 kg^{-1}) for the cooling system.

The determination of the number of stacks (n_{stack}) involved a comparison between the required propulsive power ($P_{mission}$), which is a function of the mission profile, and the net power generated by each individual stack ($P_{stack,net}$) as a function of the current and altitude, while considering the electro-mechanical efficiency of the electric motor (η_{EM}). It is important to highlight that the number of stacks is an integer derived from rounding up the value obtained through the calculation:

$$n_{stack}(j_0, h) = \frac{P_{mission}(h)}{\eta_{EM} P_{stack,net}(j_0, h)} \quad (27)$$

As initial strategy, the nominal power (i.e., maximum power) of the stack was adopted as the designed working point for the sizing of the overall propulsion system. The calculation was conducted in steady-state conditions and for two distinct on-design points within the mission profile: the cruise and the take-off. The final on-design point of the fuel cell was determined by selecting the condition with the maximum number of stacks between the two mission phases.

For the air compressor, the on-design point corresponds to the one where the maximum compression power is required. It is not guaranteed that the fuel cell's on-design point aligns with the compressor's on-design point, as the latter is mainly influenced by altitude.

The amount of hydrogen (M_{H2}, in kg) that is necessary to cover the power profile of the mission was estimated in the following way:

Table 5
Technical data of ATR72-600 [11].

ATR72-600 aircraft		
Main features		
Standard configuration	72 seats	
Engines Pratt & Whitney Canada	PW127 M/N	
Take-off power (half-wing)	1846	kW
Max cruise power (half-wing)	1590	kW
Weights		
Max take-off weight (MTOW)	22,800	kg
Structure	10,479	kg
Max payload	7550	kg
Propellers	342	kg
Kerosene-based propulsion system (2x engines + fuel + fuel system)	4429	kg
En-route performance		
Max altitude	15,000 (4600)	ft (m)

$$M_{H2} = \frac{1}{10^3 LHV_{H2}} \int_0^{t_{end}} \frac{P_{mission}(t)}{\eta_{EM}\eta_{net}(j_0, h)} dt \quad (28)$$

where $P_{mission}$ (in kW) is the mechanical power of the mission profile at time t, η_{EM} is the electromechanical efficiency of the electric motor, and η_{net} is the net efficiency of the FC system, which is a function of the operating power and the altitude. The hydrogen mass was calculated assuming a constant flow rate throughout the entire duration of the mission (two hours), and equal to the flow rate required during the cruise phase. This approximation is reasonable because the cruise phase typically occupies most of the flight time.

The cooling system was designed considering the ε-NTU method for the calculation of the required exchange area, as reported in [39]. The weight of the cooling system was subsequently determined using a gravimetric index.

In this method, some quantities need to be defined in order to proceed with the calculation, in particular the heat capacity rate for both fluids (C_i), the heat capacity rate ratio (R), the number of transfer units (NTU) and, finally, the effectiveness (ε).

The different fluid sides are characterized by their heat capacity rate for both the hot fluid (Glysantin [34]) and cold fluid (air), defined as the product of mass flow rate $(\dot{m}_i)$ and specific heat capacity (c_{p_i}):

$$C_i = \dot{m}_i c_{p_i} = \frac{Q_{tot}}{\Delta T_i} \quad (29)$$

where ΔT_i was calculated considering the inlet $(T_{in,air})$ and outlet $(T_{out,air})$ temperature of the cold fluid, and the inlet $(T_{in,coolant})$ and outlet $(T_{out,coolant})$ temperature of the hot fluid, as reported in Table 4.

The heat capacity rate ratio (R) is described as:

$$R = \frac{min\{C_i\}}{max\{C_i\}} \quad (30)$$

The number of transfer units defines a relationship between the product of the overall conductance for heat transfer (U) and the heat transfer area $(A_{cooling})$ to the minimum heat capacity rate (C_{min}) of the two fluids involved in the heat transfer:

$$NTU = \frac{UA_{cooling}}{C_{min}} \quad (31)$$

In the ε-NTU method, the effectiveness ε is defined as a measure of the thermal performance of the heat exchanger. It is a function of the number of transfer units (NTU), the heat capacity rate ratio (R) and the flow arrangement of the heat exchanger. In particular, the expression to compute ε for a counterflow heat exchanger is given by:

$$\varepsilon = \frac{1 - e^{-NTU(1-R)}}{1 - Re^{-NTU(1-R)}} \quad (32)$$

The heat exchange area was calculated based on the design value of the thermal power, imposing an effectiveness ε of 0.6 [39]. The mass flow rates of both cold and hot side were obtained considering the parameters reported in Table 4.

Finally, the overall weight of the system was assessed as the sum of the different explained contributions:

$$W_{tot} = \frac{P_{stack,max} n_{stack}}{w_{FC}} + \frac{P_{compr,max} n_{stack}}{w_{compr}} + A_{cooling} w_{cooling} + \frac{M_{H_2}}{w_{H_2 storage}} + \frac{P_{mission,TO}}{\eta_{EM} w_{EM}} \quad (33)$$

where w_i represents the gravimetric index of the component i, n_{stack} is the number of stacks, $P_{mission,TO}$ is the mechanical power of the mission profile at the take-off, and η_{EM} is the electromechanical efficiency of the motor. The values considered for the calculation are reported in Table 6.

Table 6
Gravimetric indexes for the components of the electric propulsion system.

Component	Parameter	Value	Unit
Fuel cell stack [40]	w_{FC}	3	kW kg^{-1}
Compressor [41]	w_{compr}	1.03	kW kg^{-1}
Cooling system [42]	$w_{cooling}$	1.08	kg m^{-2}
Hydrogen storage [43]	$w_{H_2 storage}$	0.12	kg_{H2} $kg^{-1}_{storage\ system}$
Electric motor [19]	w_{EM}	5.2	kW kg^{-1}

3. Results

3.1. Fitting of electrochemical model of single cell

The values of the electrochemical parameters that are part of the illustrated model were selected from the scientific literature and are summarized in Table 7. The last four parameters of the table, instead, are the result of the fitting by means of numerical methods with the aim to calibrate the model and to use it as a tool for the design.

The polarization curve was calibrated using experimental data extracted from literature. Fig. 2 illustrates the polarization curve of a PEMFC with good performance from ref. [35] (TEC36VA32 at the beginning of the lifetime, 100 % RH, 150 kPa, 80°C and 0.1 mg_{Pt}/cm^2), referred as the baseline case study in the present paper.

3.2. Efficiency curves

The system efficiency was assessed as a function of the net power output, which varies depending on the considered control volume from the stack to the system level. The resulting curves, calculated with respect to the hydrogen LHV, are reported as solid line in Fig. 3, depicting three distinct efficiency curves, as reported below.

Table 7
Input parameters for the electrochemical model fitting the MEA of ref. [35].

Electrochemical Parameters					
Fixed parameters					
Parameter	**Value**	**Unit**	**Description**		**Ref.**
b	0.03	V	Tafel slope		[26]
c_h	$7.36 \cdot 10^{-6}$	mol cm^{-3}	Oxygen concentration in the channel (p = 1 bar)		[26]
c_{ref}	$8.58 \cdot 10^{-6}$	mol cm^{-3}	Reference oxygen concentration in the channel		[26]
σ_t	0.03	S m^{-1}	Proton conductivity in the catalyst		[26]
F	96,485	C mol^{-1}	Faraday constant		[26]
l_t	0.0007	cm	CCL thickness		[35]
D_b	0.0259	cm^2 s^{-1}	Effective diffusion coefficient of GDL		[26]
V_{OC}	1.145	V	Open circuit voltage		[26]
Variable parameters					
Parameter	**Fitted value**	**Unit**	**Description**	**Range**	**Ref.**
j_*	$2.00 \cdot 10^{-3}$	A cm^{-3}	Exchange current density	$1.00 \cdot 10^{-3}$ – $4.00 \cdot 10^{-2}$	[29]
l_b	0.0312	cm	GDL thickness	0.015 – 0.04	[30]
D	$1.00 \cdot 10^{-4}$	cm^2 s^{-1}	CCL effective diffusion coefficient	$1.00 \cdot 10^{-4}$ – $3.00 \cdot 10^{-4}$	[26]
R_Ω	0.0801	Ω cm^2	Area specific resistance	0.045 – 0.2	[31]

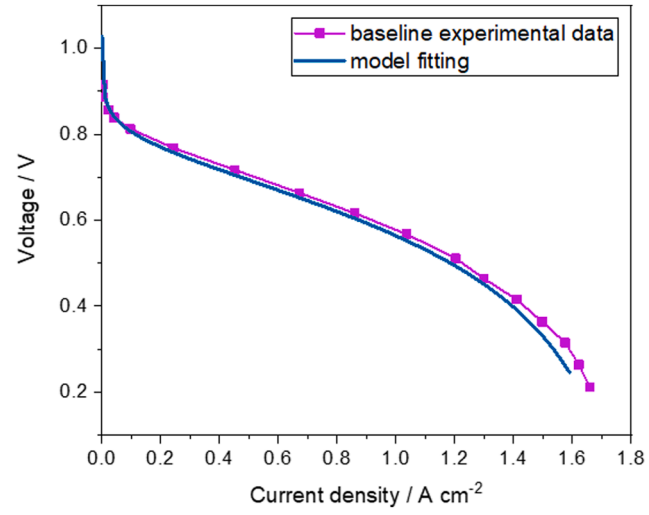

Fig. 2. Curve fitting of the baseline case study for the calibration of the PEMFC electrochemical model.

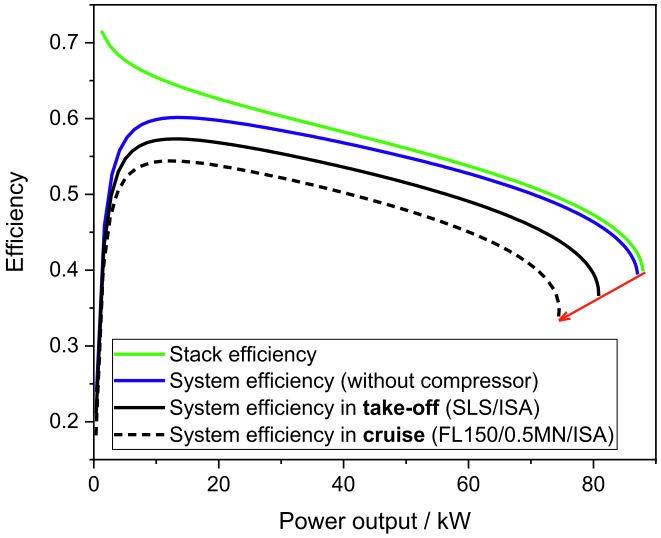

Fig. 3. Efficiencies curves as function of the power output. SLS/ISA refers to Standard Atmosphere (ISA) conditions at Sea Level (SLS) equal to 15°C and 1 bar. FL150/0.5MN/ISA refers to the atmosphere conditions at 15,000 ft of altitude and with a Mach Number (MN) of 0.5.

1. The efficiency of the stack (solid green curve), derived from the performance of the designed stack with respect to the theoretical chemical potential of the hydrogen. This efficiency decreases with an increase in current.
2. The efficiency of the system (solid blue curve), considering solely the fixed contribution of the general auxiliaries (without the air compressor). This contribution leads to a peak in the efficiency curve.
3. The efficiency of the overall fuel cell system (solid black curve), which includes the air compressor and further shifts the curve downwards.

The maximum power output varies among the three curves, following the trend indicated by the red arrow, due to different levels of BoP power requirements. While the gross power and net power align at the stack level (green curve), the net power is reduced when moving to the system level (blue and black curves). This reduction is a direct result of utilizing a portion of the stack's gross power to meet the demands of the balance of plant.

Regarding the air compressor, it is important to note that its power requirement varies with altitude, which determines different values of inlet air pressure and temperature. Consequently, the system efficiency is represented by infinite curves parametrically related to altitude. Specifically, in Fig. 3 the solid black curve was determined in the take-off phase, while the dashed black curve was calculated under the cruise conditions (highest altitude) of the present case study.

3.3. Regional aircraft scenario

3.3.1. First approach of sizing: Minimum number of stacks

First of all, the sizing point for the fuel cell system was defined through a comparison of the stack counts at two distinct design points within the mission profile: the cruise and the take-off. In the calculation, the nominal power of the stack was adopted as the designed working point. Based on these assumptions, it was finally determined that the design point corresponded to the take-off stage, consequently resulting in a power consumption at the cruise stage (off-design point) of approximately 78 % of nominal power. The results in terms of component weights are reported in Table 8.

From Fig. 4, it is evident that storage and cooling systems have a significant impact on the overall weight of the electrified system, accounting for approximately 26 % and 54 %, respectively. It is important to emphasize that the obtained value for the weight contribution of the cooling system aligns well with the literature data [11].

The sizes of both storage and cooling systems are correlated to the stack efficiency, which decreases as the working point increases. Therefore, a sensitivity analysis on the fuel cell working point was further conducted.

3.3.2. Variation of fuel cell working point

A further sensitivity analysis was conducted to determine the optimal working point of the fuel cell (w). In this phase, the efficiency curve serves as the initial tool for the optimization process. The cruise stage was selected as the reference condition for this analysis because it is associated with the longest step of the mission in terms of duration. Fig. 5 represents the system efficiency at the cruise stage, and two limiting working points were identified. The first working point, denoted in red and located to the left, provides the maximum efficiency that determines the minimum weight of the hydrogen storage. On the other hand, the second working point, depicted in blue and positioned to the right, reflects the previous sizing approach that minimizes the stack numbers and leads to a power consumption at the cruise stage equal to almost 78 % of the nominal power. To the right of the blue point, it becomes evident that the number of stacks is inadequate to meet the maximum power demand of the aircraft during take-off. Conversely, to the left of the blue point the fuel cell system starts to be oversized, resulting in a weight increase; but this trade-off is accompanied by an improvement in the system efficiency until reaching the red dot. Subsequently, moving further to the left of the red dot, the efficiency

Table 8
Results of the sizing with the approach of minimum number of stacks.

Parameter		Value	unit
Mass of H_2		446	kg
Mass of storage (LH_2 + tank)		3716	kg
Number of stacks		49	
Nominal power tot (gross)		4310	kW
Nominal power tot (net)		3691	kW
Mass of FC stacks		1437	kg
Compressor	Sizing power	628	kW
	Weight	609	kg
Cooling system	Sizing power	8725	kW
	Weight	7641	kg
Electric motor		747	kg

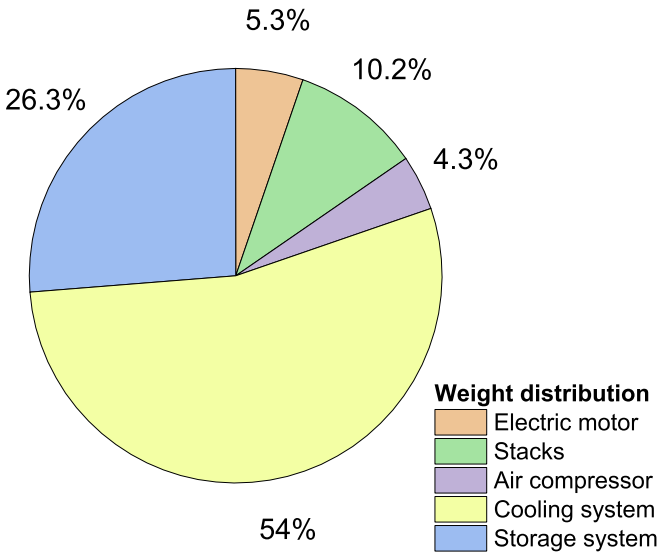

Fig. 4. Weight distribution of the components of the electrified propulsion system in the case of minimum number of stacks approach.

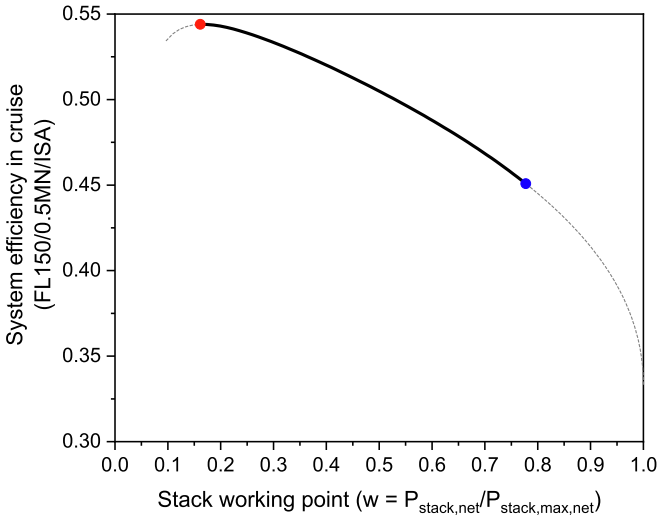

Fig. 5. System efficiency in cruise stage as function of the working point. Red dot and blue dot represent the limiting points for the optimization process.

experiences a decline, while the weight of the fuel cell system continues to increase. Operating the fuel cell system under such conditions is deemed infeasible. Hence, the optimal sizing point, which minimizes the overall weight of the propulsion system, was detected within the region situated between the two limiting points (the continuous black curve depicted in Fig. 5) during the cruise stage.

3.3.3. Optimized sizing results

The results of the calculation are here discussed and compared with the current technology. Considering that H_2 technologies in the aeronautic sector are still in their emerging state, their potential development towards future targets is assessed as well, and different scenarios are analyzed.

Table 9 shows the trend of the computed weights when imposing different options of working points of the FC system during the cruise, meaning different sizing of the FC system. In Table 9, the propulsion system weight includes the weight of the fuel cell system, the hydrogen storage and the electric motor.

The results obtained in this study reveal a noteworthy relationship between the sizing working point and the weight of the electrified propulsion system. In all examined scenarios, there is a consistent increase in the weight of the electrified propulsion system compared to the conventional kerosene-based one. However, the magnitude of this increase varies as the fuel cell is sized at different percentages of its nominal power. As can be seen in Fig. 6, for low operating points, a substantial oversizing of the number of stacks is observed, significantly impacting the overall weight of the electrified propulsion system. The weight of the stacks plays a pivotal role in determining the system's total mass at lower operating points. Conversely, for operating points near nominal conditions, the fuel cell exhibits its lowest efficiency. Consequently, the hydrogen storage and balance of plant components require larger sizes to compensate for this reduced efficiency. The optimal compromise between these two extreme conditions is found at intermediate operating points, notably at a working point of 50 %, which corresponds to approximately 64 % under on-design conditions. The analysis reveals that it is advantageous to oversize the number of stacks,

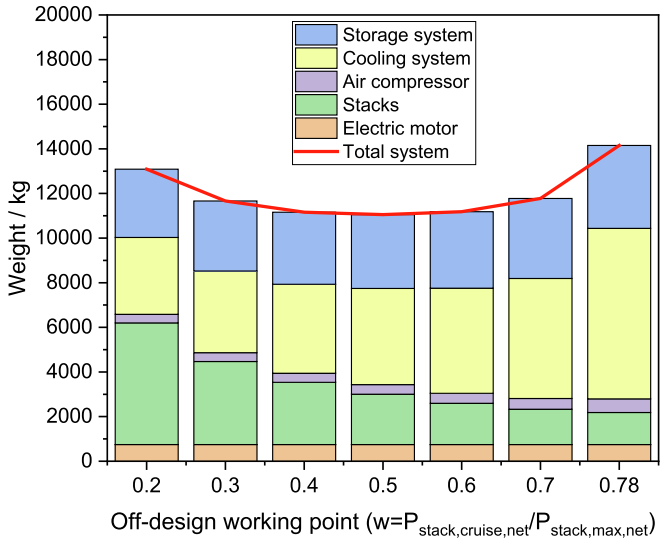

Fig. 6. Weight distribution of the components of the electrified propulsion system for different off-design working points.

Table 9
Sizing results with different working point at cruise.

Off-design working point (cruise)	System efficiency in cruise	On-design working point (take-off)	System efficiency in take-off	# stack	FC system weight, kg	H_2 Storage weight, kg	Propulsion system weight, kg	MTOW increase compared to kerosene-based aircraft
20 %	0.546	26 %	0.567	186	9278	3065	**13,091**	**38.0 %**
30 %	0.534	38 %	0.553	127	7778	3136	**11,661**	**31.7 %**
40 %	0.519	51 %	0.533	95	7185	3226	**11,158**	**29.5 %**
50 %	0.506	64 %	0.513	77	6997	3307	**11,051**	**29.0 %**
60 %	0.488	77 %	0.486	63	7006	3430	**11,183**	**29.6 %**
70 %	0.467	90 %	0.450	54	7442	3585	**11,775**	**32.2 %**
78 %	0.450	100 %	0.362	49	9687	3716	**14,150**	**42.6 %**

ensuring that even under on-design conditions, the power output from the fuel cell is lower than the nominal rating. This approach allows for operation at higher stack efficiencies, leading to a reduction in the impact of components whose size depends on stack efficiency. Specifically, the cooling system benefits from lower heat generation, the compressor operates with reduced air flow rates, and the hydrogen storage system incurs lower hydrogen consumption due to enhanced stack efficiency. The trade-off between the number of stacks and their operational efficiency adds a layer of complexity to the optimization process. Achieving the right balance becomes imperative for maximizing the benefits of electrified propulsion while addressing weight constraints.

A further step of optimization was to modify the variable electrochemical parameters by an algorithm to fit the modelled polarization curve to a high-performance experimental curve, as reported in Table 10. The latter is a polarization curve of a high-performance PEM fuel cell with the following characteristics from ref. [25]: PtCo/C cathode catalyst-based MEA, 100 % RH, 150 kPa, 80°C and 0.25 mg_{Pt}/cm^2, with the relative polarization curve shown in Fig. 7.

The fitting results were subsequently utilized as input for sizing the electrified propulsion system at various off-design working points within the previously identified range. The weight distribution is illustrated in Fig. 8, along with a comparison of the overall weight of the system, considering both the baseline PEMFC (dashed red line) and the high-performance PEMFC (solid red line).

By employing the high-performance fuel cell as referenced in [25], it becomes feasible to achieve a weight reduction at all working points compared to the baseline case. Furthermore, it is noteworthy that the condition of minimum weight is shifted to an operating point of 40 % during cruise, compared to the previous 50 %. This shift emphasizes the pivotal role of stack behavior in shaping the weight dynamics of the electrified propulsion system. In particular, comparing the polarization curves in Fig. 7, it is crucial to highlight that, while the initial segment of the high-performance polarization curve experiences slight enhancements primarily attributed to a higher platinum loading compared to the baseline case, significant performance improvements can be attained in the middle and high current density regions. These improvements are governed by resistance and mass transport phenomena, allowing for substantial enhancements through the optimization of cell parameters. At cell level, this translates to a 30 % increase in maximum electrical output of the high-performance cell compared to the baseline one.

In terms of MTOW increment, the results indicate a weight increase for the ATR72-600 aircraft ranging between 26.5 % and 37.8 % compared to the kerosene-based system. However, at the point of minimum weight, it is possible to achieve nearly 10 % reduction in the weight of the electrified system compared to the baseline case.

Table 10
Input parameters for the electrochemical model fitting the MEA of ref. [25].

Electrochemical Parameters					
Fixed parameters					
Parameter	**Value**	**unit**	**Description**		**Ref.**
b	0.03	V	Tafel slope		[26]
c_h	$7.36 \cdot 10^{-6}$	mol cm^{-3}	Oxygen concentration in the channel (p = 1 bar)		[26]
c_{ref}	$8.583 \cdot 10^{-6}$	mol cm^{-3}	Reference oxygen concentration in the channel		[26]
σ_t	0.03	S m^{-1}	Proton conductivity in the catalyst		[26]
F	96,485	C mol^{-1}	Faraday constant		[26]
l_t	0.0007	cm	CCL thickness		[35]
D_b	0.0259	cm^2 s^{-1}	Effective diffusion coefficient of GDL		[26]
V_{OC}	1.145	V	Open circuit Voltage		[26]
Variable parameters					
Parameter	**Fitted value**	**Unit**	**Description**	**Range**	**Ref.**
j_*	$1.75 \cdot 10^{-2}$	A cm^{-3}	Exchange current density	$1.00 \cdot 10^{-3}$ – $4.00 \cdot 10^{-2}$	[29]
l_b	0.0188	cm	GDL thickness	0.015 – 0.04	[30]
D	$1.40 \cdot 10^{-4}$	cm^2 s^{-1}	CCL effective diffusion coefficient	$1.00 \cdot 10^{-4}$ – $3.00 \cdot 10^{-4}$	[26]
R_Ω	0.0978	Ω cm^2	Area specific resistance	0.045 – 0.2	[31]

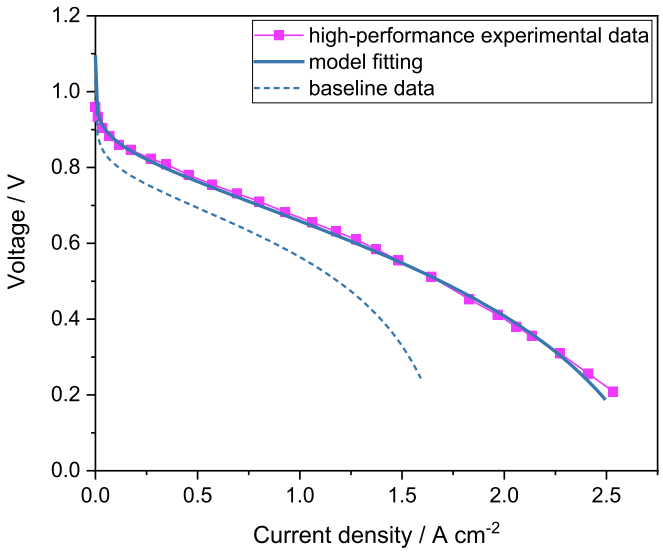

Fig. 7. Fitting of experimental high-performance PEMFC with the electrochemical model.

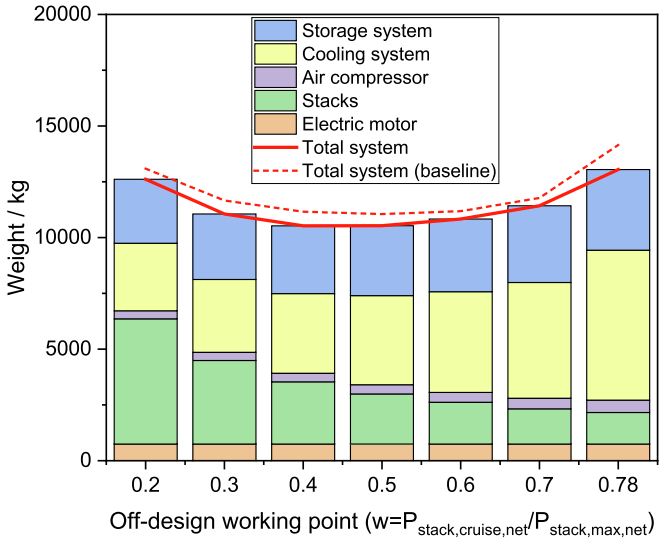

Fig. 8. Weight distribution of the components of the electrified propulsion for different off-design working points in the case of high-performance PEMFC. The dashed red line refers to the total system weight in the case of baseline PEMFC.

4. Conclusion

Hydrogen and fuel cells are currently undergoing a robust phase of development, characterized by rapid advancements in materials, integration, and manufacturing. This trend is expected to intensify, propelled by the increasing global interest in hydrogen, valued both for its inherent benefits and as a pivotal element in decarbonizing energy systems. In the transportation sector, hydrogen is emerging as a viable solution for long-distance travel, especially in high carbon footprint sectors such as air travel. For this reason, a preliminary design of a fuel cell system and a hydrogen storage system for use in aircraft was developed in this paper. An existing regional jet with its mission profile was considered as a case study. In particular, the overall weight of a hydrogen-based fuel cell system for propulsion was calculated and compared to that of the existing propulsion system. The findings reveal that the fully hydrogen-powered aircraft, employing the current technology, weighs up to 40 % more than its conventional counterpart. This weight disparity poses significant challenges to the feasibility of implementing the proposed system within the constraints of the existing aerodynamic structure.

The present work clearly illustrates that the feasibility of implementing hydrogen-based fuel cell systems depends not only on hydrogen storage capacity but also on the performance of the electrochemical cell itself. This is essential not only to reduce the required hydrogen quantities but also to mitigate the amount of heat generated during operation.

A strategy for improving the system's efficiency involves operating the fuel cell below its nominal operating point, thus oversizing the number of stacks. In fact, it was observed that a trade-off emerges between the weight of the stacks and the sizes of both storage and balance of plant. The weight of the stacks decreases with the increase of the working point, while the sizes of storage and the balance of plant components increase in tandem with the working point due to the electrochemical cell efficiency trend. As a consequence, the shift of the working point from the nominal condition has proven promising in the present study, resulting in up to 22 % system weight reduction for an on-design working point of about 64 % (of the nominal power).

Additionally, technological advancements in PEMFC offer further prospects for improving system efficiency, as demonstrated for the proposed high-performance PEMFC, which enables a weight reduction up to nearly 10 % compared to the baseline case study. Future studies should involve the optimization of the balance of plant, specifically focusing on thermal management strategies, thereby further reducing the overall system weight.

In conclusion, an integrated approach is crucial to address the complexities of interactions and scales involved, guiding progress towards efficient and implementable hydrogen technology at a regional aviation scale.

CRediT authorship contribution statement

Maria Chiara Massaro: Writing – original draft, Validation, Formal analysis, Data curation. **Simone Pramotton:** Writing – original draft. **Paolo Marocco:** Writing – review & editing, Supervision. **Alessandro Hugo Antonio Monteverde:** Writing – review & editing, Supervision, Formal analysis, Conceptualization. **Massimo Santarelli:** Writing – review & editing, Supervision.

Declaration of competing interest

The authors declare that they have no known competing financial interests or personal relationships that could have appeared to influence the work reported in this paper.

Data availability

The data that has been used is confidential.

Acknowledgments

This publication is part of the project NODES which has received funding from the MUR – M4C2 1.5 of PNRR funded by the European Union - NextGenerationEU (Grant agreement no. ECS00000036)

References

[1] International Energy Agency (IEA), "CO2 Emissions from Fuel Combustion 2017 - Highlights." [Online]. Available: www.iea.org/t&c/.
[2] Schäfer AW, et al. Technological, economic and environmental prospects of all-electric aircraft. Nat Energy 2019;4(2):160–6. https://doi.org/10.1038/s41560-018-0294-x.
[3] Y. Y. Lai *et al.*, "Analysing the opportunities and challenges for mitigating the climate impact of aviation: A narrative review," *Renewable and Sustainable Energy Reviews*, vol. 156. Elsevier Ltd, Mar. 01, 2022. doi: 10.1016/j.rser.2021.111972.
[4] European Commission. Directorate General for Mobility and Transport. and European Commission. Directorate-General for Research and Innovation., *Flightpath 2050 : Europe's vision for aviation : maintaining global leadership and serving society's needs.* Publications Office, 2011.
[5] McKinsey & Company, "Hydrogen-powered aviation – A fact-based study of hydrogen technology, economics, and climate impact by 2050," 2020. doi: https://data.europa.eu/doi/10.2843/471510.
[6] Müller C, Kieckhäfer K, Spengler TS. The influence of emission thresholds and retrofit options on airline fleet planning: an optimization approach. Energy Policy 2018;112:242–57. https://doi.org/10.1016/j.enpol.2017.10.022.
[7] Brelje BJ, Martins JRRA. Electric, hybrid, and turboelectric fixed-wing aircraft: A review of concepts, models, and design approaches. In: Progress in Aerospace Sciences. Elsevier Ltd; 2019. p. 1–19. https://doi.org/10.1016/j.paerosci.2018.06.004.
[8] Ji Z, Rokni MM, Qin J, Zhang S, Dong P. Energy and configuration management strategy for battery/fuel cell/jet engine hybrid propulsion and power systems on aircraft. Energy Convers Manag 2020;225. https://doi.org/10.1016/j.enconman.2020.113393.
[9] Baroutaji A, Wilberforce T, Ramadan M, Olabi AG. Comprehensive investigation on hydrogen and fuel cell technology in the aviation and aerospace sectors. Renew Sustain Energy Rev 2019;106:31–40. https://doi.org/10.1016/j.rser.2019.02.022.
[10] Sparano M, et al. The future technological potential of hydrogen fuel cell systems for aviation and preliminary co-design of a hybrid regional aircraft powertrain through a mathematical tool. Energy Convers Manag 2023;281. https://doi.org/10.1016/j.enconman.2023.116822.
[11] Massaro MC, Biga R, Kolisnichenko A, Marocco P, Monteverde AHA, Santarelli M. Potential and technical challenges of on-board hydrogen storage technologies coupled with fuel cell systems for aircraft electrification. J Power Sources 2023;555. https://doi.org/10.1016/j.jpowsour.2022.232397.
[12] Gnadt AR, Speth RL, Sabnis JS, Barrett SRH. Technical and environmental assessment of all-electric 180-passenger commercial aircraft. Progress Aerospace Sci. 2019;105:1–30. https://doi.org/10.1016/j.paerosci.2018.11.002. Elsevier Ltd.
[13] M. Hepperle and M. H. De, "Electric Flight-Potential and Limitations", Accessed: Nov. 30, 2023. [Online]. Available: https://elib.dlr.de/78726/1/MP-AVT-209-09.pdf.
[14] McDonald RA. Electric propulsion modeling for conceptual aircraft design. In: 52nd AIAA Aerospace Sciences Meeting - AIAA Science and Technology Forum and Exposition, SciTech 2014. American Institute of Aeronautics and Astronautics Inc.; 2014. https://doi.org/10.2514/6.2014-0536.
[15] Guida D, Minutillo M. Design methodology for a PEM fuel cell power system in a more electrical aircraft. Appl Energy 2017;192:446–56. https://doi.org/10.1016/j.apenergy.2016.10.090.
[16] Kösters TL, Liu X, Kožulović D, Wang S, Friedrichs J, Gao X. Comparison of phase-change-heat-pump cooling and liquid cooling for PEM fuel cells for MW-level aviation propulsion. Int J Hydrogen Energy Aug. 2022;47(68):29399–412. https://doi.org/10.1016/j.ijhydene.2022.06.235.
[17] Lee N, et al. Improving water management and performance of an air-cooled fuel cell system using pressurized air for aviation applications. J Electrochem Soc Aug. 2021;168(8):084503. https://doi.org/10.1149/1945-7111/ac1704.
[18] Winnefeld C, Kadyk T, Bensmann B, Krewer U, Hanke-Rauschenbach R. Modelling and designing cryogenic hydrogen tanks for future aircraft applications. Energies (Basel) 2018;11(1). https://doi.org/10.3390/en11010105.
[19] Kadyk T, Winnefeld C, Hanke-Rauschenbach R, Krewer U. Analysis and design of fuel cell systems for aviation. Energies (Basel) 2018;11(2). https://doi.org/10.3390/en11020375.
[20] Stautner W, Ansell PJ, Haran KS. CHEETA: an all-electric aircraft takes cryogenics and superconductivity on board: combatting climate change. IEEE Electrif Mag 2022;10(2):34–42. https://doi.org/10.1109/MELE.2022.3165948.
[21] E. J. Adler and J. R. R. A. Martins, "Hydrogen-powered aircraft: Fundamental concepts, key technologies, and environmental impacts," *Progress in Aerospace Sciences*, vol. 141. Elsevier Ltd, Aug. 01, 2023. doi: 10.1016/j.paerosci.2023.100922.

[22] Nicolay S, Karpuk S, Liu Y, Elham A. Conceptual design and optimization of a general aviation aircraft with fuel cells and hydrogen. Int J Hydrogen Energy 2021; 46(64):32676–94. https://doi.org/10.1016/j.ijhydene.2021.07.127.
[23] "Heaven Project WebSite." Accessed: Jan. 09, 2024. [Online]. Available: https://heaven-fch-project.eu/.
[24] "ZeroAvia." Accessed: Jan. 09, 2024. [Online]. Available: https://zeroavia.com/.
[25] D. A. Cullen *et al.*, "New roads and challenges for fuel cells in heavy-duty transportation," *Nature Energy*, vol. 6, no. 5. Nature Research, pp. 462–474, May 01, 2021. doi: 10.1038/s41560-021-00775-z.
[26] Kulikovsky AA. A physically-based analytical polarization curve of a PEM fuel cell. J Electrochem Soc 2014;161(3):F263–70. https://doi.org/10.1149/2.028403jes.
[27] M. L. Perry, J. Newman, and E. J. Cairns, "Mass transport in gas-diffusion electrodes: A diagnostic tool for fuel-cell cathodes," 1998. [Online]. Available: https://www.researchgate.net/publication/255916924.
[28] M. Eikerling and A. A. Kornyshev, "Modelling the performance of the cathode catalyst layer of polymer electrolyte fuel cells," 1998.
[29] Wang Y, Feng X. Analysis of reaction rates in the cathode electrode of polymer electrolyte fuel cell I. single-layer electrodes. J Electrochem Soc 2008;155(12): B1289. https://doi.org/10.1149/1.2988763.
[30] P. Sharma and O. P. Pandey, "Chapter 1 - Proton exchange membrane fuel cells: fundamentals, advanced technologies, and practical applications," in *PEM Fuel Cells*, Elsevier, Ed., 2022, pp. 1–24.
[31] Reshetenko T, Kulikovsky A. On the distribution of local current density along a PEM fuel cell cathode channel. Electrochem commun Apr. 2019;101:35–8. https://doi.org/10.1016/j.elecom.2019.02.005.
[32] Ballard Website, "FCgen ®-HPS Brochure." Accessed: Nov. 23, 2023. [Online]. Available: (https://www.ballard.com/docs/default-source/spec-sheets/fcgen-hps.pdf?sfvrsn=704ddd80_.
[33] National Institute of Standards and Technology, "NIST Chemistry WebBook." Accessed: Nov. 23, 2023. [Online]. Available: https://webbook.nist.gov/chemistry/.
[34] "GLYSANTIN® FC G20® ELECTRIFIED Brochure." Accessed: Nov. 23, 2023. [Online]. Available: https://www.glysantin.com/global/en.html.
[35] R. Borup and A. Weber, "2016 DOE Hydrogen and Fuel Cells Program Review FC135: FC-PAD: Fuel Cell Performance and Durability Consortium," 2020. [Online]. Available: www.fcpad.org.
[36] Qin Y, Du Q, Fan M, Chang Y, Yin Y. Study on the operating pressure effect on the performance of a proton exchange membrane fuel cell power system. Energy Convers Manag 2017;142:357–65. https://doi.org/10.1016/j.enconman.2017.03.035.
[37] Santarelli MG, Torchio MF, Calì M, Giaretto V. Experimental analysis of cathode flow stoichiometry on the electrical performance of a PEMFC stack. Int J Hydrogen Energy 2007;32(6):710–6. https://doi.org/10.1016/j.ijhydene.2006.08.008.
[38] Larminie J, Dicks A. Fuel Cell Systems Explained 2003.
[39] Link A, Ludowicy J, Staggat M. Assessment of a serial cooling concept for HTPEM fuel cell system for aviation applications. In: 33rd Congress of the International Council of the Aeronautical Sciences (ICAS); 2022.
[40] PowerCell Website, "p-stack-v-222", Accessed: Nov. 23, 2023. [Online]. Available: https://powercellgroup.com/fuel-cell-stacks/.
[41] Rotrex Website, "EK40 fuel cell compressor." Accessed: Nov. 23, 2023. [Online]. Available: https://rotrex-fuel-cell-compressor.com/fuel-cell-compressors/.
[42] Schmelcher, M., Häßy, J., 2022. Hydrogen fuel cells for aviation? A potential analysis comparing different thrust categories. ISABE 2022, 25.-30. Sep. 2022, Ottawa, Kanada.
[43] "Clean Hydrogen JU - SRIA Key Performance Indicators (KPIs)." Accessed: Nov. 30, 2023. [Online]. Available: https://www.clean-hydrogen.europa.eu/knowledge-management/strategy-map-and-key-performance-indicators/clean-hydrogen-ju-sria-key-performance-indicators-kpis_en.